

QUASISTATIC STRAIN RATES' EFFECT TO THE PROPERTIES OF ADVANCED STEELS FOR AUTOMOTIVE INDUSTRY

Emil Evin^{1)*}, Miroslav Tomáš²⁾, Marek Výrostek¹⁾

¹⁾ Technical University of Košice, Faculty of Mechanical Engineering, Department of Automotive Production, Košice, Slovakia

²⁾ Technical University of Košice, Faculty of Mechanical Engineering, Department of Computer Support of Technology, Košice, Slovakia

Received: 14.12.2015

Accepted: 25.02.2016

*Corresponding author: *emil.evin@tuke.sk*, tel.: +421 55 602 3547, Department of Automotive Production, Faculty of Mechanical Engineering, Technical University of Košice, Mäsiarska 74, 042 00 Košice, Slovakia

Abstract

The paper presents the findings of the strain rate effect, described in constitutive material models by strain rate sensitivity index m , to the strength and deformation material properties. These were evaluated from stress-strain diagrams recorded at tensile test using PC controlled testing machine TiraTEST 2300 according to STN EN ISO 6892-1. The high strength low alloyed steel H220PD, dual phase steel DP 600 and Trip steel RAK 40/70 were investigated at strain rates $\dot{\epsilon} = 0.0021, 0.083$ and 0.125 s^{-1} . The results indicate major influence of the strain rate to the strength properties while only minor influence have been found when evaluate the deformation properties. The results also shown single phase materials are more sensitive to the strain rate than dual phase materials.

Keywords: tension test, strain rate, TRIP, HSLA, mechanical properties, deformation properties

1 Introduction

Technic evolution in present is characterised by effort to increase the cars' safety and power as well as reduction of weight and emissions. This requires better understanding to the processes involved in materials when car impacts to the barrier or when components for deformation zones are produced; mainly at higher strain rates.

The cars compatibility at accident depends mainly on each car weight, structure of deformation zones and deformation properties of materials used. When car frontally impacts deformable barrier at speed lower than 20 km/h, the impact energy have to be totally absorbed in controlled manner by car-body structure and materials used for components of deformation zones to secure the passengers' safety – see **Fig. 1**. Proper car-body structure eliminates both (colored components on **Fig. 1**), the extreme deceleration or human body overloading over critical biomechanical value at first and intrusion of solid parts into the cabin at second. Thus, material properties not only for static, but also dynamic strain rates have to be known for complex analysis of car-body deformation components. The strain rate raising, resistance to deformation increases as well and some materials have shown material micro- and sub-structure change [1, 2], yield strength and deformation to fracture growth [3].

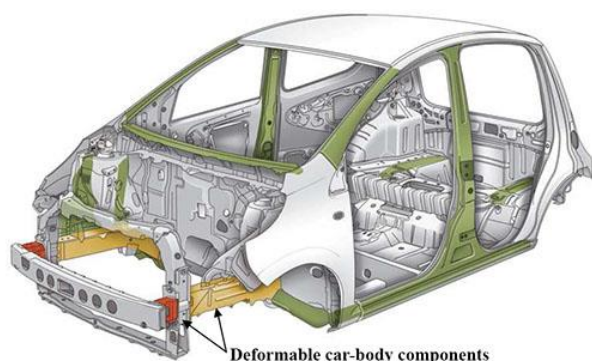


Fig. 1 Deformable car body components at frontal impact

Demands on cars' safety permanently move up, so costs for prototypes and testing arise as well. Virtual testing allows designing different structural components, using different materials, evaluating deformation characteristics of virtual prototypes in real conditions without their physical testing. Software, such as Nastran, Pam Crash, LS-Dyna etc. are used for virtual testing – **Fig. 2** [4, 5]. They allow testing each structural component individually or as a part of car-body by computer. Designers can use results solved in previous, included in databases, or make necessary changes in desired way.

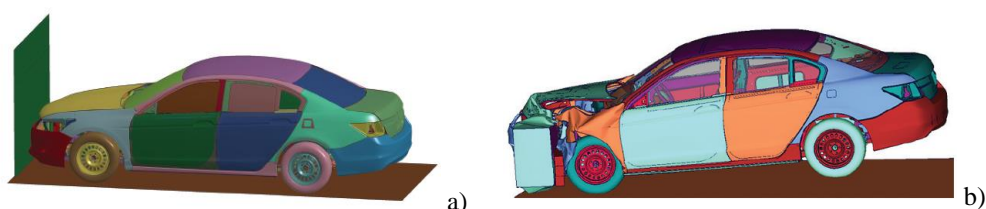


Fig. 2 Frontal impact simulation by FEM method in LS-Dyna software before a) and after crash b) [5]

Strength and deformation properties of car-body structural components when tested before production are predicted by numerical simulations. The simulation reliability depends mainly on the accuracy of input data – material properties, boundary conditions, speed, forces, etc. – not only for static but also dynamic strain rates [6]. The strain rate, when structural car-body components are deformed at crash, is derived from car speed at crash – see **Table 1**. For initial car speed 64 km/h, as defined by EuroNCAP test at frontal impact, the strain rate of car-body structural components is 155 s^{-1} [7].

Table 1 Dependence strain rate-impact velocity [7]

Impact velocity v [km/h]	0.003	0.036	0.36	3.6	9	18	36	64
Impact velocity v [m/s]	0.00083	0.01	0.1	1	2	5	10	17.78
Strain rate $\dot{\epsilon}$ [s^{-1}]	0.007	0.087	0.87	8.7	17.4	43.5	87	155

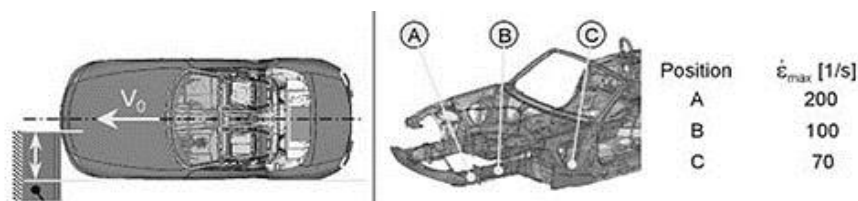


Fig. 3 The strain rate at frontal impact with 40 % overhang

Different testing equipment has to be used for material testing at different strain rates: mechanic or hydraulic testing machines offer the strain rate $< 1 \text{ s}^{-1}$, special testing equipment (VHS 8800 by Instron) offers the strain rates within 1 to 10^3 s^{-1} and specialised tests and equipment (SHPBT - Split Hopkinson Pressure Bar Test or TAT - Taylor Anvil Test) offer strain rates within 10^3 to 10^4 s^{-1} – see **Fig. 4**.

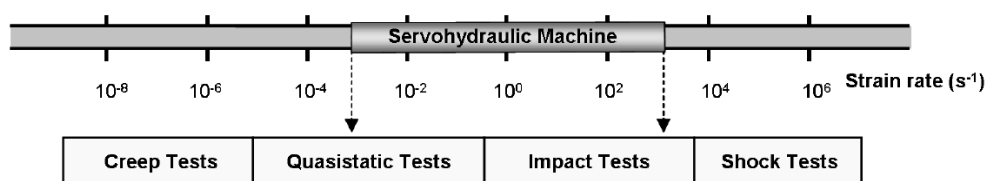


Fig. 4 Tests offering different strain rates

2 Materials and methods

The experiments were built to find out the strength and deformation properties of high strength steels – high strength low alloyed steel H220PD, Dual phase steel DP 600 and Trip steel RAK 40/70. Findings could be used for virtual crash and formability tests at different strain rates. The chemical compositions of materials used for experiment have been shown in [8].

Microstructures of experimental materials are shown on **Fig. 4** to **Fig. 6**. High strength low alloyed steel H220PD – **Fig. 5** – shows fine grained ferritic microstructure with average grain size $\cong 3 \mu\text{m}$. Secondary nitrides and carbides also have been found. Dual phase steel DP 600 – **Fig. 6** – shows ferritic-martensitic microstructure with volume content of ferrite 70 to 75 % and martensite 25 to 30 %. Some irregular martensitic islands with diameter approx. $\cong 5.8 \mu\text{m}$ have been found in ferritic matrix with average grain size $\cong 1.7 \mu\text{m}$. Martensite morphology and size wasn't possible to identify easily in many areas.

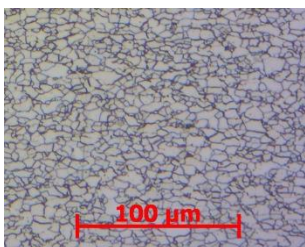


Fig. 5 Microstructure of low alloyed steel H220PD

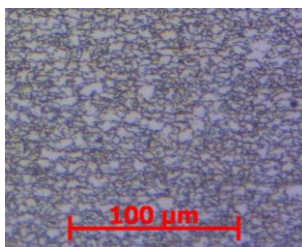


Fig. 6 Microstructure of dual phase steel DP 600

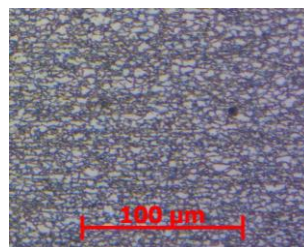


Fig. 7 Microstructure of Trip steel RAK 40/70

Trip steel RAK 40/70 – **Fig. 7** – shows ferrite, bainite and residual austenite microstructure with residual austenite volume content 5 to 10 %. Residual austenite transforms to martensite during plastic deformation, so strength and deformation work (energy absorbing ability) increase. Different structural components allow verifying not only effect of the strain rate but also structure to the deformation characteristics [8].

Most of the simulation software use constitutive material models by Hollomon, Ludwik, Swift, Voce, Krupkowski-Swift [9, 10] to define material stress-strain behaviour when deformed at static strain rates conditions. For middle and higher strain rates following constitutive material models are used [11, 12]:

- Hollomon:

$$\sigma_{qst} = K_0 \cdot \varphi^n \cdot \left(\frac{\dot{\varepsilon}}{\dot{\varepsilon}_0} \right)^m \quad (1.)$$

- Cowper-Symonds:

$$\sigma_{qst} = \sigma_0 \cdot \left[1 + \left(\frac{\dot{\varepsilon}}{D} \right)^{1/p} \right] \quad (2.)$$

- Johnson-Cook:

$$\sigma_{qst} = \left(a + b \cdot \varepsilon_i^n \right) \cdot \left(1 + C \cdot \ln \frac{\dot{\varepsilon}}{\dot{\varepsilon}_0} \right) \quad (3.)$$

where K_0 – material constant at static strain rate (reference one)

C, D – strain rate coefficients

n – strainhardening exponent

m – parameter involving sensitivity to strain rate

φ – true strain

$\dot{\varepsilon}_0$ – reference strain rate

$\dot{\varepsilon}$ – strain rate

Coefficients presenting the strain rate effect to the true stress (or deformation resistance) could be calculated from modified Hollomon constitutive equation:

$$\sigma_0 = K_0 \cdot (\dot{\varepsilon}_{0ref})^m \quad (4.)$$

If the eq. (4) is written for two different strain rates:

$$\sigma_0 = K_0 \cdot (\dot{\varepsilon}_{0ref})^m \quad (5.)$$

$$\sigma_{qst} = K_{qst} \cdot (\dot{\varepsilon}_{qst})^m \quad (6.)$$

and dividing eq. (5) to eq. (6) we reach:

$$\frac{\sigma_{qst}}{\sigma_0} = \left(\frac{\dot{\varepsilon}_{qst}}{\dot{\varepsilon}_{0ref}} \right)^m \quad (7.)$$

$$\ln \frac{\sigma_{qst}}{\sigma_0} = m \cdot \ln \frac{\dot{\epsilon}_{qst}}{\dot{\epsilon}_{0ref}} \quad (8.)$$

Then, the strain rate sensitivity index is calculated as follows:

$$m = \frac{\ln(\sigma_{qst}/\sigma_0)}{\ln(\dot{\epsilon}_{qst}/\dot{\epsilon}_{0ref})} \quad (9.)$$

The strain rates effect to the mechanical properties – yield strength R_e , ultimate tensile strength R_m , elongation A_{80} , material constant K , strainhardening exponent n and normal anisotropy ratio r – have been evaluated from stress-strain diagrams recorded at tensile test using PC controlled testing machine TiraTEST 2300 according to STN EN ISO 6892-1. The machine crosshead speed $v = 10, 300$ and $600 \text{ mm} \cdot \text{min}^{-1}$ was recalculated to the strain rate as follows:

$$\dot{\epsilon}_{10} = \frac{v}{L_0} = \frac{10 \text{ mm} \cdot \text{min}^{-1}}{80 \text{ mm}} = 0.125 \text{ min} / 60 = 0.0021 \text{ s}^{-1} \quad (10.)$$

$$\dot{\epsilon}_{300} = \frac{v}{L_0} = \frac{300 \text{ mm} \cdot \text{min}^{-1}}{80 \text{ mm}} = 3.75 \text{ min} / 60 = 0.0625 \text{ s}^{-1} \quad (11.)$$

$$\dot{\epsilon}_{600} = \frac{v}{L_0} = \frac{600 \text{ mm} \cdot \text{min}^{-1}}{80 \text{ mm}} = 7.5 \text{ min} / 60 = 0.125 \text{ s}^{-1} \quad (12.)$$

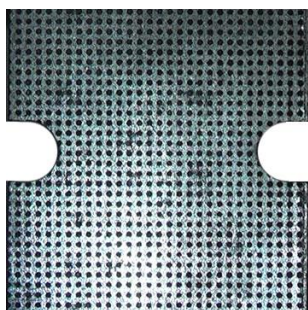


Fig. 8 Notched specimen R5 - initial state

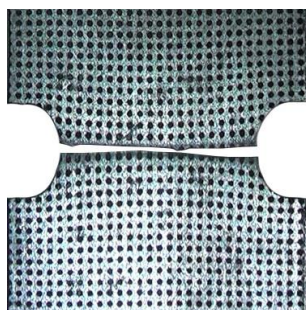


Fig. 9 Notched specimen R5 - after fracture

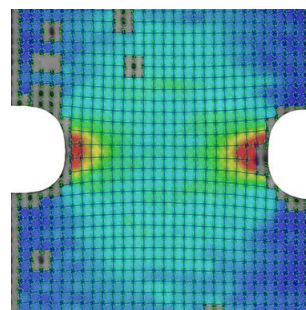


Fig. 10 Specimen R5 – major strain measured by Argus

When deformation properties and deformation work (energy absorption ability) are predicted by Finite Elements Method, forming limit curves (FLC) are other material property necessary to define. FLC allow defining the deformation scheme effect to the limit strains distribution in the sheet plane (ϕ_{1krit} , ϕ_2) and thickness (ϕ_{3krit}). The limit strains ϕ_{1krit} for assumed strain ϕ_2 have been measured by tensile test of notched specimens. The notch radii $R = 5; 15; 17.5$ and 25 mm have modelled the minor strain ϕ_2 and limit major strains ϕ_{1krit} have been evaluated. Tests have been performed on testing machine TiraTEST 2300 with crosshead speeds $v = 10, 300$ and $600 \text{ mm} \cdot \text{min}^{-1}$. Thus, strains are localised in the area defined by notch length ($L_0 = 2 \cdot R$) and it is lower than initial length 80 mm as for tensile test. Therefore, the strain rate for these specimens

have been evaluated as average value of major strain ϕ_{1krit} and time t , when the maximum load of the specimen have been reached. Limit strains in the notch root area (critical section) have been measured by 3D optical photogrammetric system Argus with grid of dots \varnothing 0.5 mm and dots' pitch 1 mm – **Fig. 8** to **Fig. 10**. Consequently, the strain rates for notched specimens were 0.047; 0.21 and 0.5 s⁻¹ when crosshead speed $v = 10$; 300 and 600 mm.min⁻¹ have been set.

3 Results and discussion

Materials have been analysed from the view of both, crash and formability virtual tests at quasistatic strain rates. The strain rate effect to the:

- strength properties – yield strength R_e and ultimate tensile strength R_m ,
- deformation properties – elongation A_{80} , uniform elongation A_g , normal anisotropy ratio r and limit strain FLD0,
- parameters of modified Hollomon constitutive equation – material constant K_0 , strainhardening exponent n and strain rate sensitivity index m ,

have been analysed. **Table 2** to **Table 4** show all measured values at different strain rates for experimental materials used, except the limit strains FLD0 shown in **Table 5**.

Table 2 Material properties of high strength low alloyed steel H220PD

Strain rate $\dot{\epsilon}$ [s ⁻¹]	Dir. / STDEV	$R_{p0.2}$ [MPa]	R_m [MPa]	A_g [%]	A_{80} [%]	$K_{0.05}$ [MPa]	$n_{0.05}$ [-]	r [-]	m [-]
0.0021	90° STDEV	388 2	449 1	17 0.6	29 0.9	728 2	0.179 0	0.659 0.004	0.019
0.0625	90° STDEV	400 8	462 0.5	17.1 0.2	27 0.4	761 2	0.186 0.001	0.659 0.006	
0.125	90° STDEV	467 8	464 0.6	18.2 0.4	27 0.3	780 1	0.195 0.001	0.659 0.006	

Table 3 Material properties of dual phase steel DP 600

Strain rate $\dot{\epsilon}$ [s ⁻¹]	Dir. / STDEV	$R_{p0.2}$ [MPa]	R_m [MPa]	A_g [%]	A_{80} [%]	$K_{0.05}$ [MPa]	$n_{0.05}$ [-]	r [-]	m [-]
0.0021	90° STDEV	376 3	632 2	19 0.2	28 0.3	1096 3	0.217 0.002	0.766 0.008	0.010
0.0625	90° STDEV	379 6	639 2	17 1	26 0.8	1116 5	0.220 0.001	0.767 0.012	
0.125	90° STDEV	393 5	640 3	17.5 0.5	25.7 0.7	1151 6	0.230 0.002	0.757 0.012	

Within the strain rate interval following material properties have increased: yield strength for low alloyed steel H220PD about 79 MPa, for dual phase steel DP 600 about 17 MPa and for Trip steel RAK 40/70 about 23 MPa; ultimate tensile strength for low alloyed steel H220PD about 15 MPa, for dual phase steel DP 600 about 8 MPa and for Trip steel RAK 40/70 about 1 MPa – see **Fig. 11** and **Fig. 12**. It has been found, the yield strength have increased more intensively than ultimate tensile strength. The finding complies with the results previously

published papers [13, 14]. The strength properties, within the quasistatic strain rates interval, increase due to lattice resistance to dislocations' movement. It is assumed, when the strain rate increases, it is not enough time to slip dislocations in planes the most properly oriented to the external loading. Thus, dislocations may also slip in planes with higher critical shear stress and consequently the higher stress is necessary to deform material [15]. The highest increase of yield strength and ultimate tensile strength has been found for low alloyed steel H220PD with fine grained microstructure created by single phase structure and precipitates. Otherwise, Trip steel RAK 40/70 shows the highest number of barriers to the dislocations' movement by slipping due to its structure created by three phases. It is assumed, the more barriers to the dislocations' movement are contained in material, the lower dependence on the strain rate material presents.

Table 4 Material properties of Trip steel RAK 40/70

Strain rate $\dot{\epsilon}$ [s ⁻¹]	Dir. / STDEV	R _{p0.2} [MPa]	R _m [MPa]	A _g [%]	A ₈₀ [%]	K _{0.05} [MPa]	n _{0.05} [-]	r [-]	m [-]
0.0021	90° STDEV	440 3	764 2	24.8 0.9	29.9 0.6	1497 2	0.3 0.001	0.658 0.020	0.011
0.0625	90° STDEV	452 0.7	761 3	22.2 0.7	28.1 0.6	1493 36	0.286 0.013	0.665 0.007	
0.125	90° STDEV	463 2	765 2	21.4 0.6	30.1 0.4	1573 1.5	0.310 0	0.684 0.007	

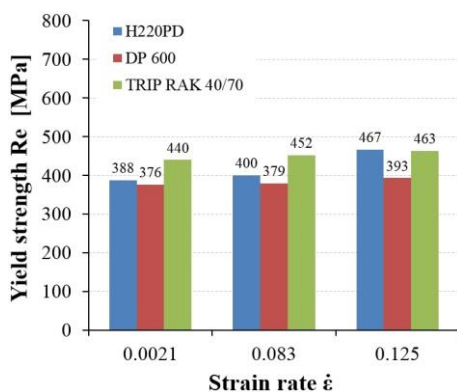


Fig. 11 Strain rate effect to the yield strength R_{p0.2}

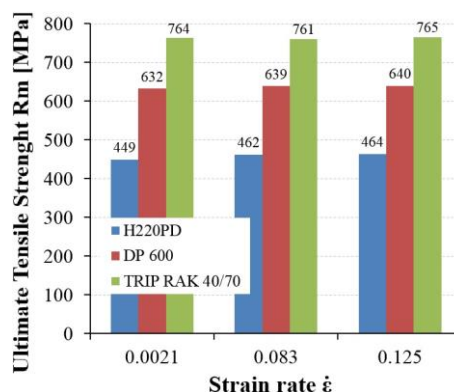


Fig. 12 Strain rate effect to the ultimate tensile strength R_m

The strain rate effect to the deformation characteristics is shown in **Fig. 13** and parameters of modified Hollomon constitutive equation is shown in **Fig. 14**. It has been found only minor influence of the strain rate variance to these material properties. The value deviations from the mean value lay within the standard deviation calculated. The finding complies to [16, 17, 18]. It is assumed, when the strain rate increases, the plastic deformation takes place in more slip planes, i.e. in direction with higher shear stress.

Measured values of limit strains FLD₀ for experimental materials show also the minor influence of the strain rate variance to the forming limit curve position. When the strain rate increases, strains are localised to the fracture area, because the more barriers to the to the dislocations'

movement, the lower difference in strain concentration onto the fracture position is. Thus, if the strain rate increases towards the critical value, any major decrease of deformation characteristics is found, but, in some cases the minor increase may even appear – **Fig. 15**.

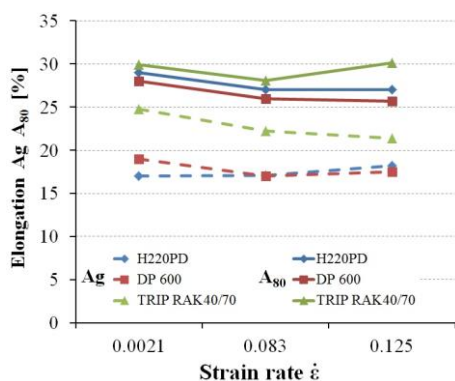


Fig. 13 Strain rate effect to the uniform Ag and total elongation A_{80}

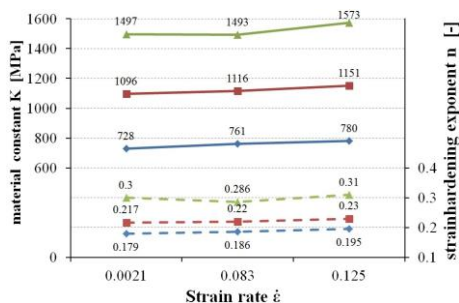


Fig. 14 Strain rate effect to material const. K and strainhardening exponent n

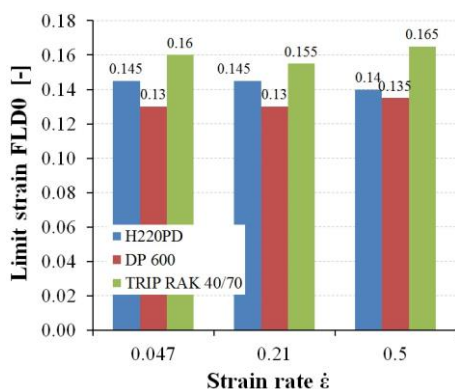


Fig. 15 Strain rate effect to the limit strain FLD0

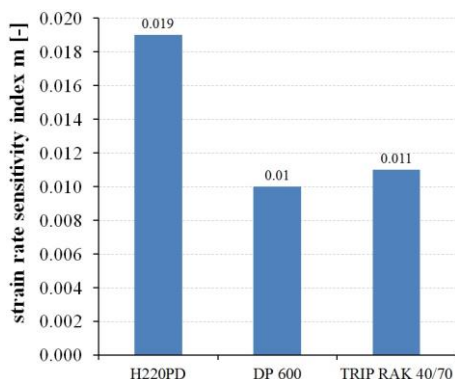


Fig. 16 Strain rate sensitivity index m calculated for experimental materials

Table 5 Limit strains FLD0 when measured for different strain rates

Strain rate $\dot{\epsilon}$ [s ⁻¹]	Dir. / STDEV	FLD0 [-]		
		H220PD	DP 600	RAK 40/70
0.047	90°	0.145	0.130	0.160
	STDEV	0.05		0.05
0.21	90°	0.145	0.130	0.155
	STDEV	0.07	0.06	0.045
0.5	90°	0.140	0.135	0.165
	STDEV	0.05	0.05	0.05

The strain rate sensitivity index m describes the strength and deformation properties sensitivity to the strain rate in complexity. The value has been determined from modified Hollomon

constitutive equation (1.), as presented in previous acc. to eq. (9.). The highest value of $m = 0.019$ has been found for low alloyed steel H220PD and the lowest one ($m = 0.01$) for dual phase steel DP 600. The strain rate sensitivity index $m = 0.011$ has been found for Trip steel RAK 40/70. Values for each experimental material are compared in **Fig. 16**. As it is shown, single phase materials are more sensitive to the strain rate as multiphase materials.

Conclusion

In the paper there are presented results of the strain rate influence to the strength and deformation properties of high strength steels: low alloyed steel H220PD, dual phase steel DP 600 and Trip steel RAK40/70. The findings have shown the strength properties are more sensitive than deformation properties, within the quasistatic strain rate interval 0.0021 s^{-1} to 0.5 s^{-1} . The yield strength has increased more than ultimate tensile strength, but the total and uniform elongation, normal anisotropy ratio neither strainhardening exponent didn't decreased.

True stress-strain curves necessary when simulating crash or formability tests by finite element method have been analysed for three quasistatic strain rates. The true stress-strain curves' sensitivity to the strain rate was described by the strain rate sensitivity index m . The highest value of index ' m ' has been found for low alloyed steel H220PD with the fine grained microstructure created by ferrite and precipitates (single phase structure). Otherwise, trip steel RAK 40/70 involves the highest number of barriers to the dislocation movement due to its three phase structure. It is supposed, the more barriers to the dislocations' movement are contained in material, the lower dependence on the strain rate material presents. The finding has to be seriously considered, if such materials are processed in automotive industry and pressure to time-shortening in stamping operations permanently increases.

The other very important material data when simulating crash or formability tests by finite element method are forming limit curves, as dependence the major strain $\phi_{1\text{krit}}$ to minor strain ϕ_2 , mainly the initial point FLD0, i.e. $\phi_{1\text{krit}}, \phi_2 = 0$. Only the minor influence of the strain rate to this material parameter has been found. The deviations laid within the standard deviation calculated and the finding complies with the results of previously published papers. It is supposed, when increase the strain rate, plastic deformation begins (dislocations' movement) also in directions with higher shear stress and it expands to other locations.

References

- [1] E. Čížmarová, J. Michel': Acta Metallurgica Slovaca, Vol. 9, 2003, No. 2, p. 90-99
- [2] J. Michel', M. Buršák: Communications, Vol. 12, 2010, No. X, p. 27-32
- [3] D. Zhu et al.: Experimental Mechanics, Vol. 51, 2011, No. 8, p.1347-1363, doi: 10.1007/s11340-010-9443-2
- [4] *Stiffness Relevance and Strength Relevance in Crash of Car Body Components* [2.12.2015] <http://autocaat.org/WebForms/ResourceDetail.aspx?id=1464#sthash.Ate4M23t.dpuf>
- [5] Ch. Liu, X. Song, J. Wang: Journal of Transportation Technologies, Vol. 4, 2014, No. 4, p. 337-342, doi: 10.4236/jtts.2014.44030
- [6] T. Pepelnjak, S. Smoljanič: RMZ – M&G, Vol. 60, 2013, No. 1, p. 3-8
- [7] R. Chvála, A. Šperková: *Ako funguje Euro NCAP (How work Euro NCAP)* [online], Bratislava, 2005 [cit. 2014 – 12 - 09]. <http://auto.sme.sk/c/2247701/ako-funguje-euro-ncap.html>
- [8] E. Evin, S. Németh, M. Tomáš: Acta Metallurgica Slovaca, Vol. 21, 2015, No. 3, p. 184-194, doi: 10.12776/ams.v21i3.603

- [9] A. Kováčová, T. Kvačkaj, R. Kočiško, J. Tiža: Acta Metallurgica Slovaca, Vol. 20, 2014, No. 3, p. 279-286, doi: 10.12776/ams.v20i3.359
- [10] P. Petroušek, T. Kvačkaj, R. Kočiško, R. Bidulský, J. Bidulská, A. Fedoriková, T. Hlava: Acta Metallurgica Slovaca, Vol. 21, 2015, No. 3, p. 176-183, doi: 10.12776/ams.v21i3.615
- [11] A. Hrivňák, E. Evin: *Formability of steel sheets*, first ed., ELFA Košice, 2004 (in Slovak)
- [12] N. K. Sanejev, V. Malik, H. S. Hebbar: International Journal of Research in Engineering and Technology, Vol. 3, 2014, No. 6, p. 98-102, doi: 10.15623/ijret.2014.0306017
- [13] M. Buršák, J. Michel': Metallurgy, Vol. 49, 2010, no. 4, p. 317-320
- [14] M. Mihaliková: Manufacturing and Industrial Engineering, Vol. 6, 2007, No. 3, p. 18-19 (in Slovak)
- [15] J. W. Martin: *Concise Encyclopedia of The Mechanical Properties of Materials*, first ed., Elsevier, 2007
- [16] J. H. Lim: Posco Technical Report, Vol. 10, 2007, No. 1, p. 116-122
- [17] S. B. Kim, H. Huh, H. H. Bok, M. B. Moon: Journal of Materials Processing Technology, Vol. 211, 2011, No. 5, p.851-862, doi:10.1016/j.jmatprotec.2010.01.006
- [18] M. Jie, C.H. Cheng, L.C. Chan, C.L. Chow: International Journal of Mechanical Sciences, Vol. 51, 2009, No. 4, p. 269-275, doi:10.1016/j.ijmecsci.2009.01.007

Acknowledgements

Authors are grateful for the support of experimental works by Slovak Research and Development Agency, under project APVV-0273-12 'Supporting innovations of autobody components from the steel sheet blanks oriented to the safety, the ecology and the car weight reduction'.